Effect of the Zeta Potential on the Corrosion Resistance of Electroless Nickel and PVDF Composite Layers Using Surfactants

Xiaochao Shen, Jiali Wang, and Gang Xin*

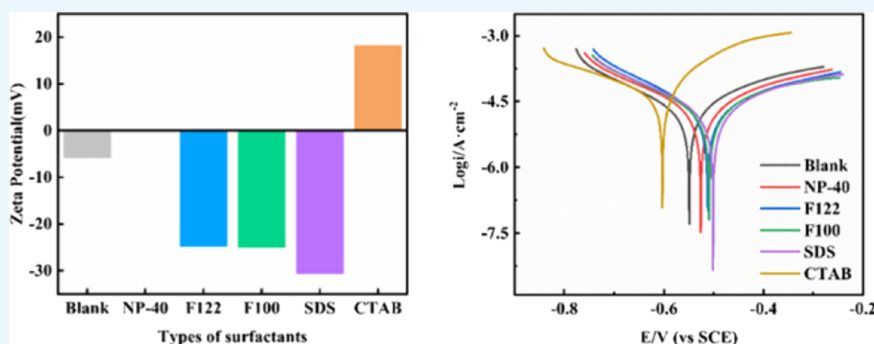Cite This: *ACS Omega* 2021, 6, 33122−33129

Read Online

ACCESS | Metrics & More | Article Recommendations | SI Supporting Information

ABSTRACT: Composite layers of Ni-P and PVDF were obtained using surfactants to enhance the corrosion resistance of the fluoride ion. The zeta potential of PVDF particles was changed with the surfactants (cationic, anionic, and nonionic). The effects of the zeta potential of PVDF particles on the particle distribution, morphology, composition, hydrophobicity, and corrosion resistance of the composite layers were studied using the different types of surfactants. The deposition behaviors of the Ni-P layer and PVDF particles strongly depended on the zeta potential of PVDF particles. Using anionic surfactants, especially $C_{12}H_{25}SO_4Na$ (SDS), the zeta potential of PVDF particles was −30.6 mV. The densification and uniformity of the composite layers with a higher amount of PVDF particles were achieved, which resulted in the superior resistance to fluoride ion corrosion. After heating at 180 °C, the PVDF particles were melted, spread, and filled into the pores of the composite layers, which led to the further enhanced corrosion resistance. It was demonstrated that the zeta potential of PVDF particles affected the dispersion, stability, and codeposition with electroless nickel, which resulted in the uniform and dense composite layers and enhanced the corrosion resistance of the fluoride ion.

1. INTRODUCTION

A Ni-P composite layer with enhanced wear resistance, high temperature resistance, and corrosion resistance was obtained by adding second-phase particles into the Ni-P matrix, such as Al_2O_3, SiC, MoS_2, polytetrafluoroethylene (PTFE), or polyvinylidene fluoride (PVDF).[1−4] There were two key steps in the deposition process of the Ni-P composite layer, i.e., Ni^{2+} ions discharged on the substrate surface to form the Ni-P layer and second-phase particles embedded in the Ni-P layer to form the composite layer. During this process, the uniform distribution of particles in the Ni-P layer and the tightness with the Ni-P layer were the key factors affecting the properties of the Ni-P composite layer. However, the particles would agglomerate in electroless plating solution due to van der Waals forces,[5] surface electrostatic charge, gravity, high surface energy,[6,7] and so on. The aggregates of the second-phase particles resulted in the particles being nonuniformly dispersed in the layer, affecting its due particle effect. In the current research, the dispersing methods of second-phase particles in the plating bath were investigated, such as mechanical treatment,[8,9] surface modification,[10,11] adding

surfactants,[12−15] and so on. Surfactants had been widely used because they could improve the surface properties, change the particle interaction, improve the surface wettability, and avoid reaggregation between particles.[16,17] The addition of surfactants would have an effect on the features of the Ni-P layer and the number of embedded particles, which was mainly related to the zeta potential of particles that adsorbed the surfactants. The literature focused heavily on the effects of surfactants on the surface morphology, the content of second-phase particles, and the corrosion resistance of the layer. Afroukhteh et al.[14] studied the effect of adding different surfactants on the content of TiC in Ni-P-TiC layers, and the results showed that the TiC content was the highest in the layers using anionic surfactants.
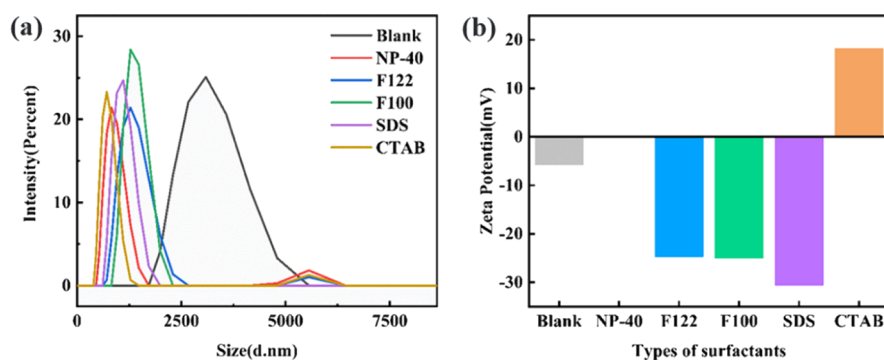
Figure 1. Changes in PVDF particles' (a) size and (b) zeta potential with the addition of different surfactants.

Chen et al.[15] showed that anionic surfactants (SDBS) further improved the corrosion resistance of Ni-P-nanoAl$_2$O$_3$ composite layers under optimal conditions, while the addition of cationic surfactants resulted in poorer corrosion resistance. However, there were few studies relating to the effect of the change of the zeta potential of the second-phase particles on the deposition behavior of the composite layers caused by the addition of different surfactants in the bath. Some polymer materials could be miscible, such as poly(vinyl ester)s and polyacrylates,[18] poly(styrene-co-acrylonitrile) and poly(phenyl acrylate) or poly(vinyl benzoate),[19] poly(phenyl acrylate) and poly(styrene-co-acrylonitrile),[20] etc. The thermodynamic compatibility between them could be elaborated from the perspective of the Flory−Huggins interaction parameter.[21] A layer of the Ni-P alloy deposited on the surface of polymer materials such as ABS[22] and PP[23] would improve its corrosion resistance, wear resistance, magnetic shielding, and other functions. Polymer materials were also added to Ni-P alloys to improve wear resistance, corrosion resistance, self-lubrication, and anti-sticking properties.[1,2,24,25] The formation of an intermetallic layer between the Ni-P composite layer and the steel substrate after heat treatment improved substrate−coating adhesion.[26] At the same time, the layer changed phase at the corresponding temperature, and the hardness, adhesion, and corrosion resistance of the layer were enhanced.[17,25,27] Huang et al.[25] showed that the phase transition from an amorphous Ni-P matrix to a mixture of polycrystalline Ni and Ni$_3$P alloys occurred at around 340 °C. The highest microhardness and best adhesion properties were observed for the samples annealed at 400−450 °C for 1 h. Moreover, PVDF has good hydrophobicity, corrosion resistance, high temperature resistance, dielectric properties, and other special properties, which make it worthwhile to thoroughly investigate the codeposition of PVDF particles and the Ni-P layer.[7]

In this work, Ni-P-PVDF composite layers were prepared by electroless plating. The zeta potential of PVDF particles changed by using surfactants (cationic, anionic, and nonionic), and the effect of heat treatment on the corrosion resistance of composite layers was investigated, which would provide a theoretical basis for the application of Ni-P composite layers.

2. RESULTS AND DISCUSSION

2.1. Particle Size and Zeta Potential Determination.
The large specific surface area and surface energy led to PVDF particles in a state of energy instability, resulting in agglomeration.[6,7] The aggregated PVDF particles were difficult to be captured by the Ni-P pores due to their large size and weight and sinking.[15] The addition of surfactants was found to promote the deagglomeration of particles and make the particles more uniformly dispersed in the plating solution.[3,15,28,29]

The surface tension decreased to varying degrees with the addition of different surfactants (Figure S1). In terms of reducing the surface tension of the bath, fluorosurfactants (F100 and F122) had the strongest ability since fluorine atoms were very difficult to be polarized, making the fluorocarbon chain less polar than the hydrocarbon chain. Because of the low polarity of the fluorocarbon chain, the hydrophobic effect of the fluorocarbon chain was much stronger than that of the hydrocarbon chain, and the mutual molecular force was weak so that it had a stronger ability to reduce surface tension.

The stability of particles in a suspension was determined by the particle size and zeta potential.[13,30] Figure 1 shows the particle size distribution and the zeta potential of PVDF particles in the baths without any surfactants and baths containing different surfactants. As presented in Figure 1a, in a bath without any surfactants, we could observe aggregates with a diameter of 3 μm, and the peak was very broad, which indicated the uneven dispersion of PVDF. In the baths containing different surfactants, the aggregates of PVDF with a diameter of 1.2 μm could be observed. Meanwhile, the peaks were very narrow, which indicated that the surfactant promoted the deagglomeration of the PVDF particles in the plating bath.[28] It could be seen from Figure 1a that there were PVDF aggregates of about 5.6 μm in the blank bath. The PVDF particles dispersed with cationic or nonionic surfactants used had a bimodal particle size distribution[30] with average sizes of around 1.2 and 5.6 μm, respectively. The existence of small peaks of about 5.6 μm indicated that the PVDF aggregates were not completely depolymerized. The PVDF particles dispersed with an anionic surfactant had a unimodal particle size distribution and were more homogeneous (as indicated by a narrower peak). In the solution containing NP-40, the zeta potential of PVDF particles was −0.00580 mV, so they had strong attraction to each other, indicating poor dispersity. However, in Figure 1a, the PVDF particles were well-dispersed, even better than those of F100 and F122. This was because before the experiment, we carried out ultrasonic treatment of the solution so that the particles could be further dispersed through the cavitation effect.[31] Therefore, the final dispersion effect of PVDF particles in solution was not only related to their surface charge but also related to ultrasonic dispersion. At the same time, when we measured the particle size in the static state after ultrasonic treatment, the particles in the solution might agglomerate again.[32]

The zeta potential was a factor of suspension and dispersion stability of solid particles in the bath.[13] If the absolute values of the zeta potential of all particles in the bath were large, then they would tend to repel each other, and thus, the particles were not easily agglomerated. Figure 1b shows the variation of the zeta potential of PVDF particles at various surfactants. At pH 4.5, the zeta potential of PVDF particles in the bath without any surfactants was found to be −5.75 mV, showing that the PVDF particles were negatively charged (due to adsorption of $H_2PO_2^-$ ions on the surface) at these experimental conditions. Because the electrostatic repulsive forces were small near the PVDF particles, the van der Waals attractive forces made particles aggregate and agglomerate.[13]

The addition of the ionic surfactant caused the zeta potential of PVDF particles toward the more positive or more negative direction, and PVDF particles got better dispersion by increasing the electrostatic repulsion between particles. Since the hydrophilic group of the cationic surfactant molecule (CTAB) was positively charged, the zeta potential of the PVDF particles increased from −5.75 to +18.2 mV after the addition of CTAB. Since the hydrophilic group of the anionic surfactant molecule was negative, the zeta potential of the PVDF particles was changed to a more negative direction after the addition of the anionic surfactant. It is well-known that the larger the absolute value of the zeta potential was, the more stable the particles were and the easier the particles mixed in the Ni-P matrix.[15,17] As presented in Figure 1b, the zeta potential of the PVDF particles dropped from −5.75 to −30.6 mV after the addition of the anionic surfactant (SDS), which meant that the bath of the addition of SDS could maintain a more stable state during the deposition process.

The hydrophobic end of the nonionic surfactant molecule was adsorbed on the PVDF particles, and the hydrophilic end entered the aqueous phase to form a thicker hydration film, which acted as a spatial resistance, and generated entropy repulsive forces to disperse the PVDF particles. The zeta potential of the PVDF particles increased from −5.75 to −0.00580 mV after the addition of the nonionic surfactant (NP-40). Apparently, NP-40 screened the negative charge of PVDF particles. However, the zeta potential of the PVDF particles dropped from −5.75 to −24.7 mV after the addition of the nonionic surfactant (F122). This might be because of the fluorine atoms containing strong electrical negative properties in F122.

2.2. Morphology and Composition of the Layers. To examine the role of different surfactants, in this study, Ni-P-PVDF composite layers with 1 g/L PVDF in the bath were selected as the research model, and the surface morphologies are shown in Figure 2.
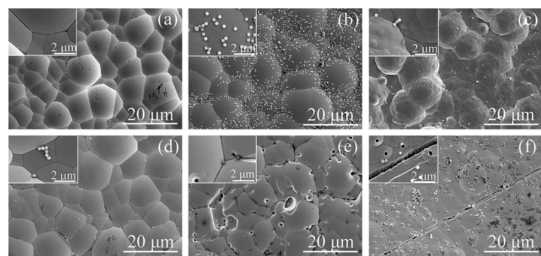
Figure 2a shows that the Ni-P plating layer exhibited a typical cauliflower-like structure. The grain boundary was obvious, and the grains were not uniform in size, which illustrated that the Ni-P plating layer was amorphous.[15,33] It could also be seen from the XRD diagram (Figure S2) that all layers had a broad peak at 45°, indicating that all layers were amorphous. At a higher magnification as shown in Figure 2a, a few micropores were observable for the Ni-P plating layer, which might be due to the slow hydrogen evolution during the electroless deposition of Ni-P.[6,23] From an overall perspective, the composite layers became denser and more homogeneous after the addition of the surfactant. This was due to the fact that the surfactant could reduce the surface tension between the surface of the hydrogen bubble and the surface tension between the substrate and the hydrogen bubble. Therefore, the captured hydrogen stayed on the substrate surface for a short time and easily left the substrate surface. However, Table 1

Table 1. The Deposition Rate and Layer Composition with Dependence on Different Surfactants

| surfactant | Ni-P | Ni-P-PVDF | | | | |
	blank	SDS	F100	NP-40	F122	CTAB
deposition rate (μm/h)	5.20	3.90	3.72	4.20	3.95	1.38
Ni (wt %)	88.26	84.42	87.31	87.17	87.53	85.40
P (wt %)	8.67	8.60	8.72	8.82	8.77	9.24
PVDF (wt %)		2.39	1.25	1.06	1.08	1.84

shows that the deposition rates of the Ni-P-PVDF composite layers added to different surfactants were smaller than that of the Ni-P layer. This might be due to the fact that the surfactants and PVDF particles covered a portion of the active site on the substrate, thereby reducing the deposition rate.[1,14,24,34]

It could be proven by Figure S3 that the particles in the coating were PVDF particles, and the diameter of a single molecule was about 350 nm. Most of the plating layers of Figure 2b−f show a uniform distribution of single PVDF particles (about 350 nm), and only a minor portion of 1 μm was distributed in the layers, which did not correspond to the PVDF particle size (an average particle diameter of 1.2 μm) in Figure 1. This indicated that PVDF particles excluded large aggregates during the deposition process.[29,30,35] The surfaces of the composite layers added to the anionic surfactants (Figure 2b,c) were denser, wherein the amount of PVDF particles in the composite layer with the addition of SDS (2.39%) was the highest (Table 1). The hydrophobic end of the anionic surfactant molecule was adsorbed on PVDF particles, while the hydrophilic end pointed to the plating solution,[28] resulting in the combination of Ni^{2+} ions, thereby forming a Stern layer around it to produce a Stern potential. $H_2PO_2^-$ ions were attracted to the Stern layer, which in turn attracted more Ni^{2+} ions to form an ionic cloud around PVDF particles. When reaching the surface of the catalytic substrate, the Ni^{2+} and $H_2PO_2^-$ ions located on the outer surface of the ion cloud around the PVDF particles were reduced to Ni and P atoms and entered the catalytic surface. Since the matrix was rich in Ni^{2+} ions, it was easier for negative PVDF particles to adsorb on the surface of the Ni-P plating layer by electrostatic interaction. Figure 2f presents the FESEM picture of the composite layer with a cationic surfactant (CTAB). The grain refinement, cracks, and holes consistent with PVDF particles

Figure 2. Surface morphology of (a) Ni-P layer and Ni-P-PVDF composite layers plated from baths with different surfactants: (b) SDS, (c) F100, (d) NP-40, (e) F122, and (f) CTAB.

were present on the layer. Meanwhile, the percentage of PVDF in the layer was 1.84%, the content of P increased, the content of Ni decreased, and the deposition rate of the layer was minimum (Table 1). Since the cationic surfactant was opposite to the surface of the PVDF particles, it first neutralized the negative charge of the surface of the PVDF particles. The PVDF particles generated in electrical neutralization would adsorb the second layer of cationic surfactant ions to make PVDF particles positively charged and then dispersed PVDF particles by electrostatic repulsion. During the experimental process, the second layer of cationic surfactants wrapped in the surface of the PVDF particles was reacted with $H_2PO_2^-$ ions such that PVDF particles were incorporated into the plating layer. The hydrophobic chain of the first layer of cationic surfactants wrapped by PVDF particles in the layer was located on the outside, which might make the PVDF particles in the layer easily washed away by the flowing bath and hydrogen generated in the experiment to form pores. The crack in the composite layer with CTAB addition (Figure 2f) might be caused by the increase in internal stress between the composite layer and the substrate.

The content of PVDF particles in the composite layers with nonionic surfactants was less (Table 1), and there were pores (Figure 2e). The hydrophobic end of the nonionic surfactant molecule was adsorbed on PVDF particles, and the hydrophilic end entered the aqueous phase to form a thick hydration film, which acted as a steric hindrance and produced entropy repulsion to disperse the PVDF particles. The thick hydration film weakened the interaction between PVDF particles and Ni^{2+}, $H_2PO_2^-$, and the substrate, which hindered the codeposition of PVDF particles leading to fewer PVDF particles being incorporated into the Ni-P layer. The absolute value of the zeta potential of PVDF in the bath with F122 was larger (Figure 1b), which led to the greater and uniform dispersion of PVDF particles, so the particles easily entered the Ni-P layer during the experiment. However, the PVDF particles in the layer were easily washed out by the flowing bath and hydrogen generated by the experiment, so it was difficult to codeposit with the Ni-P layer. Therefore, it would lead to the decrease in the content of PVDF in the layer and the appearance of holes.

Figure 3 shows the cross-sectional FESEM images of the Ni-P layer and Ni-P-PVDF composite layers with different
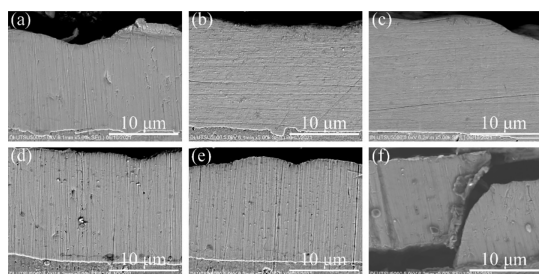

Figure 3. Cross-sectional FESEM images of (a) Ni-P layer and Ni-P-PVDF composite layers plated from baths with different surfactants: (b) SDS, (c) F100, (d) NP-40, (e) F122, and (f) CTAB.

surfactants. The successful binding of PVDF particles into the layers could be seen in Figure 3b−f, in which the composite layers with anionic and nonionic surfactants were uniform, and they were well-combined with the steel matrix without cracks. However, the adhesion between the Ni-P-

PVDF composite layer with the cationic surfactant and the steel substrate was poor, resulting in cracks, which was consistent with the discovery shown in Figure 2f.

2.3. Contact Angle. Water contact angles of the Ni-P layer and Ni-P-PVDF composite layers made from the different surfactant baths are shown in Figure 4. Obviously, the contact
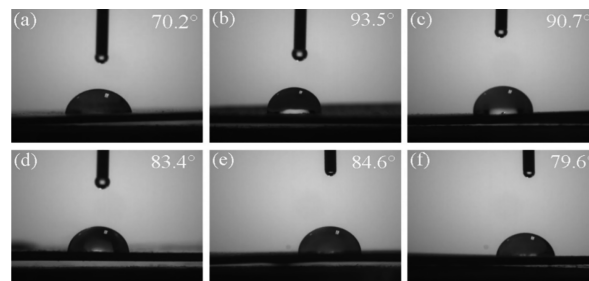

Figure 4. Contact angle measurement of (a) Ni-P layer and Ni-P-PVDF layers with different surfactants: (b) SDS, (c) F100, (d) NP-40, (e) F122, and (f) CTAB.

angles of the Ni-P-PVDF composite layers were greater than that of the Ni-P layer, which was due to the hydrophobicity of PVDF particles in the composite layers. The contact angles of the composite layers with anionic surfactants were the largest, which was due to the largest content of hydrophobic PVDF particles in the layer (Table 1). Because the content of PVDF particles in the composite layer with nonionic surfactants was less (Table 1) and there were holes on the surface, the measured contact angles were smaller than those of the composite layers with anionic surfactants. The contact angle of the layer with cationic surfactants was not much larger than that of the Ni-P layer. Since there were holes and cracks in the layer, even if the content of PVDF particles in the layer was high (Table 1), the contact angle of the layer was still very small. The degree of hydrophobicity of the surface would affect the polarization resistance of the surface; the stronger the hydrophobicity, the greater the polarization resistance and the higher the corrosion resistance, which could be confirmed in the following electrochemical experiments.[36]

2.4. Corrosion Resistance. The corrosion resistance of the layers was evaluated by the electrochemical method. The polarization curves of the Ni-P layer and Ni-P-PVDF composite layers with different surfactants in 0.01 mol/L NH_4HF_2 solution are shown in Figure 5. According to the
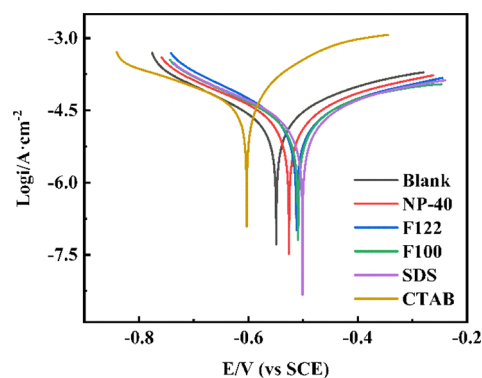

Figure 5. Potential polarization curves of the Ni-P layer and Ni-P-PVDF layers with different surfactants after immersing in 0.01 mol/L NH_4HF_2 solution.

polarization curve, the corrosion current density (I_{corr}) and the corrosion rate of different samples were fitted by the Tafel extrapolation method, and the corresponding electrochemical data are shown in Table 2. The corrosion potential (E_{corr}),

Table 2. Corrosion Parameters of the Ni-P Layer and Ni-P-PVDF Layers with Different Surfactants

sample	E_{corr}/V (vs SCE)	I_{corr}/μA·cm^{-2}	CR/mm·a^{-1}
blank	−0.54905	9.8	0.1133
NP-40	−0.52574	9.1	0.1059
F122	−0.51181	9.2	0.1067
F100	−0.50908	8.5	0.0991
SDS	−0.50105	8.4	0.0971
CTAB	−0.60303	30.1	0.3494

corrosion current density (I_{corr}), and corrosion rate of the Ni-P layer were −0.54905 V, 9.8 μA/cm^2, and 0.1133 mm/a, respectively. It was obvious from Table 2 that the Ni-P-PVDF composite layers with anionic or nonionic surfactants had higher corrosion potentials and lower corrosion current densities and corrosion rates than the Ni-P layer. This indicated that the Ni-P-PVDF composite layers with anionic or nonionic surfactants had better corrosion resistance than the Ni-P layer in 0.01 mol/L NH$_4$HF$_2$ solution. The corrosion resistance of the Ni-P-PVDF composite layer with the anionic surfactant was the best. First of all, the surfactant could reduce the surface tension between the hydrogen bubble and the plating solution and between the substrate and the hydrogen bubble. Therefore, on the substrate surface, the captured H$_2$ stayed for a shorter time and left the surface easily, resulting in fewer pores in the layer and a denser layer. Second, the density of the layer was increased, and the time for the corrosion ion like F$^-$ to reach the substrate was prolonged; thus, the corrosion resistance of the layer was improved.[15,37] In addition, PVDF particles were inert and had very low electrical conductivity. The uniform distribution of PVDF particles with strong hydrophobicity in the layer would enhance the hydrophobicity of the layer and hinder the contact between the corrosion medium and the layer, thus improving the corrosion resistance of the layer.[28]

However, the Ni-P-PVDF composite layer with the cationic surfactant had a more negative corrosion potential and a higher corrosion current density and corrosion rate than the Ni-P layer, which indicated that its corrosion resistance was worse than that of the Ni-P layer. This was due to voids and cracks in the Ni-P-PVDF composite layer with cationic surfactants (Figure 2f), which had a negative impact on corrosion resistance by creating conductive pathways for the electrolyte to infiltrate into the layer.

Figure 6 shows the Nyquist plots of the Ni-P layer and Ni-P-PVDF layers with different surfactants immersed in 0.01 mol/L NH$_4$HF$_2$ solution. As could be seen in Figure 6, the Nyquist curves of all layers show a single semicircle in the frequency range studied, which indicated that the corrosion process of the layer involved a single time constant and the dissolution process was controlled by the charge transfer reaction.[14,38] Compared with the Ni-P layer, the shape of the Nyquist curve of Ni-P-PVDF composite layers did not change, which indicated that the addition of PVDF particles and surfactants did not change the corrosion mechanism of the Ni-P layer.[15] However, the shapes of these Nyquist curves were similar while different in size, which indicated that different surfactants
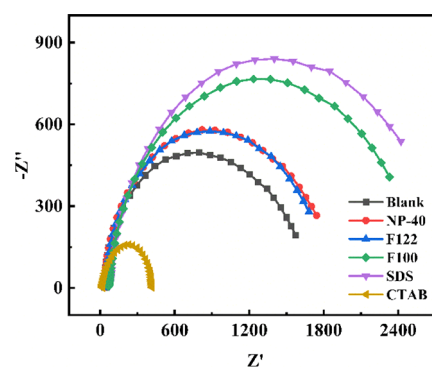

Figure 6. Nyquist plots of the Ni-P layer and Ni-P-PVDF layers with different surfactants immersed in 0.01 mol/L NH$_4$HF$_2$ solution.

would affect the corrosion resistance of Ni-P-PVDF composite layers. The EIS spectra were checked by fitting the equivalent circuit model, which is shown in Figure 7.
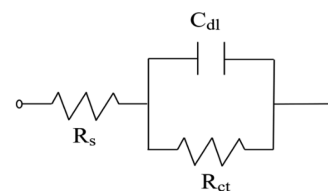

Figure 7. Equivalent circuit model used to fit the EIS data.

Figure 7 shows an equivalent circuit consisting of a solution resistance (R_s), a charge transfer resistance (R_{ct}), and an electrical double-layer capacitance at the interface of the electrode and the electrolyte (C_{dl}).[14,28,38,39] The fitting results are shown in Table 3. The change in the charge transfer

Table 3. EIS Fitting Results of the Ni-P Layer and Ni-P-PVDF Layers with Different Surfactants after Being Immersed in 0.01 mol/L NH$_4$HF$_2$ Solution

samples	R_s (Ω·cm^2)	C (μF·cm^{-2})	R_{ct} (Ω·cm^2)
blank	4.474	25.16	1462
NP-40	3.579	24.94	1657
F122	4.660	35.87	1623
F100	7.358	22.32	2226
SDS	7.815	30.49	2436
CTAB	2.927	34.82	372

resistance (R_{ct}) value could be attributed to some extent to the change in layer density. The higher the layer density and the larger the R_{ct}, the more difficult the charge transfer between the layer and the solution. The denser layer could better inhibit the diffusion of O$_2$ and corrosion media from the external solution to the substrate through pores or crevices.[39] The charge transfer resistance R_{ct} of the composite layer with the cationic surfactant decreased, which indicated that the corrosion resistance of the composite layer was not as good as that of the Ni-P layer. The charge transfer resistance (R_{ct}) of the composite layers with anionic surfactants was the highest, which showed that the layers were uniform and compact and had the strongest corrosion resistance.

2.5. The Effect of Heat Treatment. The melting point of PVDF was about from 170 to 185 °C. The Ni-P-PVDF composite layer from SDS was treated at 160, 180, and 200 °C

for 2 h. The changes in the surface morphology and corrosion resistance of the composite layer were observed and studied.

Figure 8 shows the FESEM diagrams of the Ni-P-PVDF composite layers after heat treatment. The PVDF particles
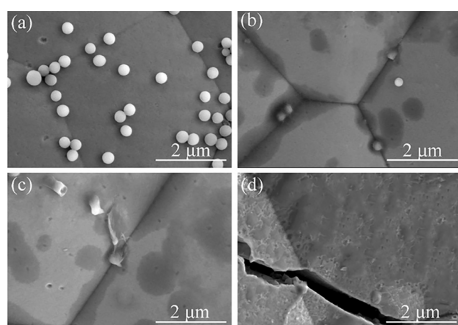

Figure 8. Surface morphology of Ni-P-PVDF layers with SDS added after heat treatment: (a) untreated, (b) 160, (c) 180, and (d) 200 °C.

were partly melted at 160 °C. At 180 °C, the PVDF particles mainly melted, spread, and filled into the pores. However, cracks appeared in the composite layers at 200 °C, which were caused by the unequal expansion of PVDF particles and the Ni-P layer.[39]

Figure 9 shows the polarization curves of Ni-P-PVDF composite layers after heat treatment at 160, 180, and 200 °C.
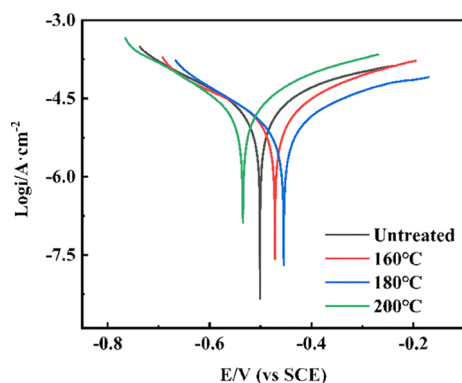

Figure 9. Potential polarization curves of Ni-P-PVDF layers with SDS added after heat treatment after immersing in 0.01 mol/L NH_4HF_2 solution: (a) untreated, (b) 160, (c) 180, and (d) 200 °C.

The corrosion resistance of the composite layer was optimal after heat treatment at 180 °C, and the melted PVDF particles were filled into the pores, which made the layer more compact and resist fluoride ions infiltrating into the layer and reacting with the substrate. However, the corrosion resistance decreased at 200 °C due to the cracks appearing (Table 4).

Table 4. Corrosion Parameters of Ni-P-PVDF Layers with SDS after Heat Treatment

	E_{corr}/V (vs SCE)	I_{corr}/μA·cm^{-2}	CR/mm·a^{-1}
untreated	−0.50105	8.4	0.0971
160 °C	−0.47172	6.7	0.0774
180 °C	−0.45447	5.1	0.0524
200 °C	−0.53456	9.7	0.1131

3. CONCLUSIONS

The effect of the zeta potential on the fluorine ion corrosion resistance of Ni-P and PVDF composite layers using the different surfactants was investigated. The zeta potential of PVDF particles was changed by adsorbing different surfactants. A more negative zeta potential was beneficial to dispersing of the PVDF particles and stability of the plating baths, which further affected the codeposition of PVDF particles and Ni-P layers. The Ni-P-PVDF composite layers from anionic surfactants presented the optimal resistance to fluoride ion corrosion, which were dense and uniform. After heat treatment at 180 °C, the PVDF particles were melted and filled into the pores, which made the layer more compact and enhanced the corrosion resistance for fluorine ions.

4. EXPERIMENTS

4.1. Preparation of the Substrates. Q235 steel sheets, sized 50 × 20 × 0.5 mm, were used as substrates. The steel sheets were initially polished with waterproof emery papers from 400 to 1500 grit systematically and degreased in alkaline solution for 30 min. Afterward, they were immersed in 10% HCl solution for 30 s to dislodge the oxide film and activate the surface.

4.2. Bath Composition and Operating Conditions. The basic chemical plating solution formulas are illustrated in Table S1 of the Supporting Information. The surfactants used in the experiment are presented in Table 5. The surfactant (0.2

Table 5. Surfactants Used in This Study

type	surfactant	code name
cationic	$C_{19}H_{42}BrN$	CTAB
anionic	$C_{12}H_{25}SO_4Na$	SDS
	$C_{15}H_4OF_{17}SO_3R$	F100
nonionic	$C_{15}H_{24}O\cdot(C_2H_4O)_n$	NP-40
	$C_{12}H_5OF_{17}\cdot(C_2H_4O)_n$	F122

g/L) was added to the solution before electroless nickel deposition, and PVDF powders of 350 nm diameter were added in the above solution at a concentration of 1 g/L and ultrasonically dispersed for 30 min. This bath worked at pH 4.5 and 90 °C. The respective time was adjusted according to the deposition rate of different surfactants (Table 1) to prepare the same thickness layer. The composite layer was optimized and heat-treated at 160, 180, and 200 °C for 2 h.

4.3. Characterization. The particle size distribution and the zeta potential of PVDF particle suspensions were measured by a ZS90 nanoparticle size and zeta potential analyzer in solutions with and without the presence of surfactants. The surface morphology of the layers was observed with an SU5000 thermal field emission scanning electron microscope (FESEM), while an Ultim Max energy spectrum analyzer of the British Oxford company (EDXA) was relied upon for analysis of their composition. The water contact angle of the layers was measured by a JCD2000D2W contact angle measuring instrument.

4.4. Electrochemical Experiments. The corrosion resistance properties of the layers were analyzed by potentiodynamic polarization and electrochemical impedance spectroscopy (EIS) techniques in 0.01 mol/L NH_4HF_2 solution using a GS350 electrochemical workstation. A conventional three-electrode system was used with a platinum wire as the auxiliary electrode, a saturated calomel electrode as

the reference electrode, and coated steel (with an exposed surface area of 1 cm^2) as the working electrode. Potentiodynamic polarization tests were performed in the range of −0.25 to +0.25 V SCE at a constant scan rate of 5 mV/s. The corrosion potential (E_{corr}) and the corrosion current density (I_{corr}) of each layer were obtained by Tafel curve epitaxy. The EIS measurements were carried out in the frequency range of 100 kHz to 10 mHz, accompanied by a 5 mV amplitude disturbance.

■ ASSOCIATED CONTENT

Ⓢ Supporting Information

The Supporting Information is available free of charge at https://pubs.acs.org/doi/10.1021/acsomega.1c05490.

Chemical composition of the electroless plating, surface tension of baths, XRD patterns of layers, and SEM image of PVDF particles (PDF)

■ AUTHOR INFORMATION

Corresponding Author

Gang Xin − *Faculty of Chemical, Environmental and Biological Science and Technology, Dalian University of Technology, Dalian 116024, China;* Ⓞ orcid.org/0000-0001-5127-2346; Phone: 13841130165; Email: gxin@dlut.edu.cn

Authors

Xiaochao Shen − *Faculty of Chemical, Environmental and Biological Science and Technology, Dalian University of Technology, Dalian 116024, China*

Jiali Wang − *Faculty of Chemical, Environmental and Biological Science and Technology, Dalian University of Technology, Dalian 116024, China*

Complete contact information is available at:
https://pubs.acs.org/10.1021/acsomega.1c05490

Notes

The authors declare no competing financial interest.

■ ACKNOWLEDGMENTS

■ REFERENCES

(1) Mafi, I. R.; Dehghanian, C. Comparison of the coating properties and corrosion rates in electroless Ni−P/PTFE composites prepared by different types of surfactants. *Appl. Surf. Sci.* **2011**, *257*, 8653−8658.

(2) Ankita, S.; Singh, A. Corrosion and wear resistance study of Ni-P and Ni-P-PTFE nanocomposite coatings. *Open Eng.* **2011**, *1*, 234−243.

(3) Abdoli, M.; Sabour Rouhaghdam, A. Preparation and characterization of Ni−P/nanodiamond coatings: Effects of surfactants. *Diamond Relat. Mater.* **2013**, *31*, 30−37.

(4) Afroukhteh, S.; Dehghanian, C.; Emamy, M. Preparation of electroless Ni−P composite coatings containing nano-scattered alumina in presence of polymeric surfactant. *Prog. Nat. Sci.: Mater. Int.* **2012**, *22*, 318−325.

(5) Nwosu, N.; Davidson, A.; Hindle, C.; Barker, M. On the Influence of Surfactant Incorporation during Electroless Nickel Plating. *Ind. Eng. Chem. Res.* **2012**, *51*, 5635−5644.

(6) Rabizadeh, T.; Allahkaram, S. R. Corrosion resistance enhancement of Ni−P electroless coatings by incorporation of nano-SiO$_2$ particles. *Mater. Des.* **2011**, *32*, 133−138.

(7) Kang, G.-d.; Cao, Y.-m. Application and modification of poly(vinylidene fluoride) (PVDF) membranes − A review. *J. Membr. Sci.* **2014**, *463*, 145−165.

(8) Zhao, Q.; Tan, S.; Xie, M.; Liu, Y.; Yi, J. A study on the CNTs-Ag composites prepared based on spark plasma sintering and improved electroless plating assisted by ultrasonic spray atomization. *J. Alloys Compd.* **2018**, *737*, 31−38.

(9) Yazdani, S.; Tima, R.; Mahboubi, F. Investigation of wear behavior of as-plated and plasma-nitrided Ni-B-CNT electroless having different CNTs concentration. *Appl. Surf. Sci.* **2018**, *457*, 942−955.

(10) Razmjou, A.; Mansouri, J.; Chen, V. The effects of mechanical and chemical modification of TiO$_2$ nanoparticles on the surface chemistry, structure and fouling performance of PES ultrafiltration membranes. *J. Membr. Sci.* **2011**, *378*, 73−84.

(11) Shi, F.; Ma, Y.; Ma, J.; Wang, P.; Sun, W. Preparation and characterization of PVDF/TiO$_2$ hybrid membranes with ionic liquid modified nano-TiO$_2$ particles. *J. Membr. Sci.* **2013**, *427*, 259−269.

(12) Jiang, C.-c.; Cao, Y.-k.; Xiao, G.-y.; Zhu, R.-f.; Lu, Y.-p. A review on the application of inorganic nanoparticles in chemical surface coatings on metallic substrates. *RSC Adv.* **2017**, *7*, 7531−7539.

(13) Zielinska, K.; Stankiewicz, A.; Szczygiel, I. Electroless deposition of Ni-P-nano-ZrO$_2$ composite coatings in the presence of various types of surfactants. *J. Colloid Interface Sci.* **2012**, *377*, 362−367.

(14) Afroukhteh, S.; Dehghanian, C.; Emamy, M. Corrosion behavior of Ni−P/nano-TiC composite coating prepared in electroless baths containing different types of surfactant. *Prog. Nat. Sci.: Mater. Int.* **2012**, *22*, 480−487.

(15) Chen, Y.; Hao, Y.; Huang, W.; Ji, Y.; Yang, W.; Yin, X.; Liu, Y.; Ling, X. Corrosion behavior of Ni-P-nano-Al$_2$O$_3$ composite coating in the presence of anionic and cationic surfactants. *Surf. Coat. Technol.* **2017**, *310*, 122−128.

(16) Matsuda, H.; Nishira, M.; Kiyono, Y.; Takano, O. Effect of Surfactants Addition on the Suspension of PTFE Particles in Electroless Plating Solutions. *Trans. IMF* **2017**, *73*, 16−18.

(17) Chang, C.-S.; Hou, K.-H.; Ger, M.-D.; Chung, C.-K.; Lin, J.-F. Effects of annealing temperature on microstructure, surface roughness, mechanical and tribological properties of Ni−P and Ni−P/SiC films. *Surf. Coat. Technol.* **2016**, *288*, 135−143.

(18) Rana, D.; Mandal, B. M.; Bhattacharyya, S. N. Analogue Calorimetric Studies of Blends of Poly(vinyl ester)s and Polyacrylates. *Macromolecules* **1996**, *29*, 1579−1583.

(19) Rana, D.; Mandal, B. M.; Bhattacharyya, S. N. Analogue calorimetry of polymer blends: poly(styrene-co-acrylonitrile) and poly(phenyl acrylate) or poly(vinyl benzoate). *Polymer* **1996**, *37*, 2439−2443.

(20) Rana, D.; Mandal, B. M.; Bhattacharyya, S. N. Miscibility and phase diagrams of poly(phenyl acrylate) and poly(styrene-co-acrylonitrile) blends. *Polymer* **1993**, *34*, 1454−1459.

(21) Rana, D.; Bag, K.; And, S. N. B.; Mandal, B. M. Miscibility of poly(styrene-co-butyl acrylate) with poly(ethyl methacrylate): Existence of both UCST and LCST. *J. Polym. Sci., Part B: Polym. Phys.* **2000**, *38*, 369−375.

(22) Tang, X.; Bi, C.; Han, C.; Zhang, B. A new palladium-free surface activation process for Ni electroless plating on ABS plastic. *Mater. Lett.* **2009**, *63*, 840−842.

(23) Rao, L.; Tang, J.; Hu, S.; Shen, L.; Xu, Y.; Li, R.; Lin, H. Inkjet printing assisted electroless Ni plating to fabricate nickel coated polypropylene membrane with improved performance. *J. Colloid Interface Sci.* **2020**, *565*, 546−554.

(24) Tsai, S.-Y.; Lin, C.-H.; Jian, Y.-J.; Hou, K.-H.; Ger, M.-D. The fabrication and characteristics of electroless nickel and immersion Au-

polytetrafluoroethylene composite coating on aluminum alloy 5052 as bipolar plate. *Surf. Coat. Technol.* **2017**, *313*, 151−157.

(25) Huang, Y. S.; Zeng, X. T.; Hu, X. F.; Liu, F. M. Heat treatment effects on EN-PTFE-SiC composite coatings. *Surf. Coat. Technol.* **2005**, *198*, 173−177.

(26) Liew, K. W.; Kong, H. J.; Low, K. O.; Kok, C. K.; Lee, D. The effect of heat treatment duration on mechanical and tribological characteristics of Ni−P−PTFE coating on low carbon high tensile steel. *Mater. Des.* **2014**, *62*, 430−442.

(27) Wu, Y.; Liu, H.; Shen, B.; Liu, L.; Hu, W. The friction and wear of electroless Ni−P matrix with PTFE and/or SiC particles composite. *Tribol. Int.* **2006**, *39*, 553−559.

(28) Nayana, K. O.; Ranganatha, S.; Shubha, H. N.; Pandurangappa, M. Effect of sodium lauryl sulphate on microstructure, corrosion resistance and microhardness of electrodeposition of Ni−Co₃O₄ composite coatings. *Trans. Nonferrous Met. Soc. China* **2019**, *29*, 2371−2383.

(29) Liu, Y.; Zhao, Q. Effects of surfactants on the PTFE particle sizes in electroless plating Ni-P-PTFE coatings. *Trans. IMF* **2003**, *81*, 168−171.

(30) Amell, A.; Muller, C.; Sarret, M. Influence of fluorosurfactants on the codeposition of ceramic nanoparticles and the morphology of electroless NiP coatings. *Surf. Coat. Technol.* **2010**, *205*, 356−362.

(31) Sumitomo, S.; Koizumi, H.; Uddin, M. A.; Kato, Y. Comparison of dispersion behavior of agglomerated particles in liquid between ultrasonic irradiation and mechanical stirring. *Ultrason. Sonochem.* **2018**, *40*, 822−831.

(32) Nguyen, V. S.; Rouxel, D.; Hadji, R.; Vincent, B.; Fort, Y. Effect of ultrasonication and dispersion stability on the cluster size of alumina nanoscale particles in aqueous solutions. *Ultrason. Sonochem.* **2011**, *18*, 382−388.

(33) Yoon, J.-W.; Koo, J.-M.; Kim, J.-W.; Ha, S.-S.; Noh, B.-I.; Lee, C.-Y.; Park, J.-H.; Shur, C.-C.; Jung, S.-B. Effect of boron content in electroless Ni−B layer on plating layer properties and soldering characteristics with Sn−Ag solder. *J. Alloys Compd.* **2008**, *466*, 73−79.

(34) Ger, M.-D.; Hwang, B. J. Effect of surfactants on codeposition of PTFE particles with electroless Ni-P coating. *Mater. Chem. Phys.* **2002**, *76*, 38−45.

(35) Jang, H. J.; Kim, R. H.; Kwon, H. S.; Kim, T. S.; Cho, K. C.; Choi, J. S.; Heo, T. Y.; Lee, J. H. Study on corrosion resistance of gas cylinder materials in HF, HCl and HBr environments. *Corros. Eng., Sci. Technol.* **2013**, *44*, 445−452.

(36) Vazirinasab, E.; Jafari, R.; Momen, G. Application of superhydrophobic coatings as a corrosion barrier: A review. *Surf. Coat. Technol.* **2018**, *341*, 40−56.

(37) Mohammadi, M.; Ghorbani, M. Wear and corrosion properties of electroless nickel composite coatings with PTFE and/or MoS₂ particles. *J. Coat. Technol. Res.* **2011**, *8*, 527−533.

(38) Shabani-Nooshabadi, M.; Ghandchi, M. S. Santolina chamaecyparissus extract as a natural source inhibitor for 304 stainless steel corrosion in 3.5% NaCl. *J. Ind. Eng. Chem.* **2015**, *31*, 231−237.

(39) Eivaz Mohammadloo, H.; Sarabi, A. A.; Mohammad Hosseini, R.; Sarayloo, M.; Sameie, H.; Salimi, R. A comprehensive study of the green hexafluorozirconic acid-based conversion coating. *Prog. Org. Coat.* **2014**, *77*, 322−330.